

# Hot Gas in the Circumstellar Bubble S 308

You-Hua Chu<sup>1</sup>, Martín A. Guerrero<sup>1,2</sup>, Robert A. Gruendl<sup>1</sup>, Guillermo García-Segura<sup>3</sup>,  
Heinrich J. Wendker<sup>4</sup>

## ABSTRACT

S 308 is a circumstellar bubble blown by the WN4 star HD 50896. It is one of the only two single-star bubbles that show detectable diffuse X-ray emission. We have obtained *XMM-Newton* EPIC observations of the northwest quadrant of S 308. The diffuse X-ray emission shows a limb-brightened morphology, with a clear gap extending from the outer edge of the diffuse X-ray emission to the outer rim of the nebular shell. The X-ray spectrum of the diffuse emission is very soft, and is well fitted by an optically thin plasma model for a N-enriched plasma at temperatures of  $\sim 1.1 \times 10^6$  K. A hotter gas component may exist but its temperature is not well constrained as it contributes less than 6% of the observed X-ray flux. The total X-ray luminosity of S 308, extrapolated from the bright northwest quadrant, is  $\leq (1.2 \pm 0.5) \times 10^{34}$  ergs s<sup>-1</sup>. We have used the observed bubble dynamics and the physical parameters of the hot interior gas of S 308 in conjunction with the circumstellar bubble model of García-Segura & Mac Low (1995) to demonstrate that the X-ray-emitting gas must be dominated by mixed-in nebular material.

*Subject headings:* ISM: bubbles — ISM: individual (S 308) — stars: winds — stars: Wolf-Rayet — stars: individual (HD 50896) — X-rays: individual (S 308)

## 1. Introduction

Fast winds from massive stars can interact with their ambient medium and blow bubbles. The physical structure of a bubble in a homogeneous interstellar medium (ISM) has been

---

<sup>1</sup>Astronomy Department, University of Illinois, 1002 W. Green Street, Urbana, IL 61801; chu@astro.uiuc.edu, mar@astro.uiuc.edu, gruendl@astro.uiuc.edu

<sup>2</sup>Now at Instituto de Astrofísica de Andalucía (CSIC), Spain; mar@iaa.es

<sup>3</sup>Instituto de Astronomía-UNAM, Apartado Postal 877, Ensenada, 22800 Baja California, México; ggs@astrosen.unam.mx

<sup>4</sup>Hamburger Sternwarte, Gojenbergsweg 112, Hamburg, D-21029 Germany; h.j.wendker@hs.uni-hamburg.de

modeled by Weaver et al. (1977). In their model of a pressure-driven bubble, the shocked fast wind reaches temperatures of  $10^7$ – $10^8$  K and forms a contact discontinuity with the cool ( $10^4$  K), dense shell of swept-up ambient medium. Heat conduction and mass evaporation across this interface lowers the temperature and raises the density of the hot interior gas, producing  $10^5$ – $10^6$  K gas that can be observed at ultraviolet and X-ray wavelengths.

Of all known bubbles blown by single massive stars, only two show detectable diffuse X-ray emission: NGC 6888 and S 308 (Bochkarev 1988; Wrigge, Wendker, & Wisotzki 1994; Wrigge 1999). *ROSAT* PSPC and *ASCA* SIS observations of NGC 6888 showed a limb-brightened X-ray morphology and spectra that were best fitted by a dominant component at  $1.5 \times 10^6$  K and a weaker component at  $8 \times 10^6$  K (Wrigge et al. 1994, 1998, 2003). *ROSAT* PSPC observations of S 308 detected X-ray emission near the shell rim, but detailed analysis was hampered by the low surface brightness and the obstruction of the PSPC window support structure projected near the shell rim (Wrigge 1999).

Both NGC 6888 and S 308 have Wolf-Rayet (WR) central stars and show enhanced N and He abundances in the nebulae, suggesting that they consist of stellar material ejected by the central stars during the red supergiant (RSG) phase (Esteban et al. 1992). If the RSG mass loss rate was constant, the density of the circumstellar material would fall off with a  $r^{-2}$  dependence, where  $r$  is the radius. The formation and evolution of a bubble blown in such a circumstellar medium has been calculated analytically by García-Segura & Mac Low (1995), and numerically simulated by García-Segura, Langer, & Mac Low (1996) specifically for WR central stars with RSG progenitors.

Wrigge et al. (1998, 2003) modeled the diffuse X-ray emission from NGC 6888 by incorporating Weaver et al.’s (1977) heat conduction in the analytical solution of García-Segura & Mac Low (1995), and found that the model could not explain simultaneously the observed limb-brightened morphology, surface brightness, and the presence of a high temperature component. By reducing the efficiency of heat conduction at the interface, it was possible to reproduce the limb-brightened morphology but not the surface brightness.

The recently launched *XMM-Newton Observatory* has unprecedented sensitivity in the soft X-ray band, and thus provides an excellent opportunity to observe the hot gas in bubble interiors. We have obtained *XMM-Newton* observations of S 308. This paper reports our analysis of this new X-ray observation and discusses the implications of our results on the physical structure of S 308’s hot interior.

## 2. XMM-Newton Observations of S 308

S 308 was observed with the *XMM-Newton Observatory* on 2001 October 23-24, in Revolution 343, using the EPIC/MOS1, EPIC/MOS2, and EPIC/pn CCD cameras (Observation ID 79570201). The two EPIC/MOS cameras were operated in the full-frame mode for a total exposure time of 47.0 ks, and the EPIC/pn camera in the extended full-frame mode for 43.0 ks. For all observations, the medium optical blocking filter was used. The angular resolution of the EPIC cameras at energies below 1 keV is  $\sim 6''$ , and the energy resolutions of the EPIC/MOS and EPIC/pn CCDs are 60 eV and 100 eV at 1 keV, respectively (Dahlem 1999; Strüder et al. 2001).

We received the *XMM* pipeline products, and processed them further using the *XMM-Newton* Science Analysis Software (SAS version 5.3.3) and the calibration files from the Calibration Access Layer available on 2002 October 22. The event files were screened to eliminate bad events, such as those due to charged particles. For the EPIC/MOS observations, only events with CCD patterns 0–12 (similar to *ASCA* grades 0–4) were selected; for the EPIC/pn observation, only events with CCD pattern 0 (single pixel events) were selected. As the background directly affects the detectability of diffuse X-ray emission, periods of high background have to be excluded. We assessed the background by binning the data over 100 s time intervals for each instrument in the 10–12 keV energy band; the background was considered high if the count rates were  $\geq 0.3$  cnts  $s^{-1}$  for the EPIC/MOS or  $\geq 1.5$  cnts  $s^{-1}$  for the EPIC/pn. Unfortunately, 15 ks after the observation of S 308 started, a high-background flare occurred and persisted throughout the rest of the observation. The useful exposure times were thus reduced to 22.7 ks and 16.9 ks for the EPIC/MOS and EPIC/pn observations, respectively.

## 3. Spatial Distribution of Diffuse X-ray Emission from S 308

We have observed only the bright northwest quadrant of S 308 because the field-of-view of the EPIC cameras is smaller than the angular extent of the bubble. To produce an X-ray image of S 308, we first extract images in the 0.25–1.15 keV energy band from the EPIC/pn and EPIC/MOS observations individually, then mosaic these three images together to increase the S/N ratio and to reduce the null exposure in the gaps between CCDs. This energy band includes all photons detected from S 308, as shown later in §4. The images are sampled with a pixel size of  $2''$ , which is adequate for the resolution of EPIC cameras. The mosaicked raw EPIC image is presented in Fig. 1a. This image is adaptively smoothed with Gaussian profiles of FWHM ranging from  $2''$  to  $50''$ , and divided by a normalized exposure map to remove the telescope and instrument sensitivity variations across the field. The

resultant image is presented in grey scale with contours in Fig. 1b.

Diffuse X-ray emission from S 308 is clearly detected, and a limb-brightened morphology is seen. To compare the distribution of diffuse X-ray emission to the cool nebular shell, we present an [O III]  $\lambda 5007$  line image of S 308 from Gruendl et al. (2000) in Fig. 1c, and plot the X-ray contours extracted from the smoothed EPIC image over the [O III] image in Fig. 1d. The diffuse X-ray emission is completely interior to the optical shell. An apparent gap exists between the outer edge of the diffuse X-ray emission and the outer rim of the optical shell. Close inspection shows bright optical filaments delineating the brightest X-ray-emitting regions. It is not clear whether the gap between the outer edge of the X-ray and optical emission regions is caused by a lack of X-ray emission or additional absorption from the nebular shell.

The optical shell of S 308 shows a protrusion in the northwest corner, suggesting a blowout. This is a very mild case of blowout because its X-ray edge recedes the farthest from the optical shell edge, unlike the superbubble N44’s blowout where the diffuse X-ray emission extends beyond the optical shell (Chu et al. 1993).

#### 4. Physical Properties of the Hot Gas in S 308

The physical properties of the hot gas in S 308 can be determined by modeling the observed X-ray spectrum. We have extracted spectra from the event files of the three EPIC cameras separately, using a source aperture outlined in Fig. 1a, and a background aperture exterior to S 308 but with a similar area,  $\sim 210$  arcmin $^2$ . Small regions encompassing X-ray point sources are excised from the source and background apertures. For illustration, regions around the point sources within the source aperture are marked in Fig. 1a. The background-subtracted, vignetting-corrected spectra binned by a constant channel width of 15 eV are displayed in Fig. 2. The EPIC/pn and EPIC/MOS spectra show similar shapes, but the EPIC/pn camera is more sensitive and has detected a larger number of counts,  $7,900 \pm 150$  cnts. We have thus concentrated on the EPIC/pn spectrum for further analysis and discussion.

The EPIC/pn spectrum of S 308 is very soft, peaking at the He-like triplet of N VI at 0.42–0.43 keV and declining sharply toward higher energies. Above 0.7 keV, the spectrum shows only possibly weak emission at  $\sim 0.92$  keV, corresponding to the He-like triplet of Ne IX; no emission is detected beyond 1.0 keV. The presence of line features suggests thermal plasma emission; therefore, we have used the MEKAL optically-thin plasma emission model (Kaastra & Mewe 1993; Liedahl, Osterheld, & Goldstein 1995) to simulate the X-

ray spectrum of S 308. The observed spectrum is simulated by passing the MEKAL model spectrum through an interstellar absorption with cross-sections from Balucińska-Church & McCammon (1992) and convolving it with the EPIC/pn response matrices. The simulated spectra are compared to the observed spectrum in the 0.3–2.0 keV range. The best-fit model, judged by the  $\chi^2$  statistics, gives the plasma temperature, volume emission measure, and foreground absorption.

The input parameters for the spectral fitting include the temperature and abundances of the emitting plasma, and the column density and abundances of the foreground absorbing medium. It is impractical to allow all these parameters to vary freely in the spectral fits because the spectral resolution is limited and the number of photons detected is modest. We have therefore used independently determined information to constrain the model parameters and fix them whenever possible. First, we adopt the solar abundances for the foreground absorbing material, since S 308 is at a distance of  $1.5 \pm 0.3$  kpc.<sup>5</sup> Next we consider the abundances of the X-ray-emitting plasma. While the hot gas contains shocked fast stellar wind, its mass may be dominated by nebular material evaporated across the conduction front or ablated by the fast stellar wind (Weaver et al. 1977; Pittard, Dyson, & Hartquist 2001a; Pittard, Hartquist, & Dyson 2001b). Thus, we start the spectral fits using the nebular abundances of S 308. For He, O, N, and Ne, we adopt the abundances determined from optical spectrophotometry by Esteban et al. (1992). For Mg and Fe, we assume that their abundances relative to the solar values are tied to that of O. The C abundance of the nebula is unknown, although the N/C abundance ratio of the fast wind has been determined to be 14 within a factor of 3 uncertainty (Hillier 1988). We adopt a 0.1 solar abundance for C, which is somewhat arbitrary but compatible with the stellar wind abundances. The final abundances of C, N, O, Ne, Mg, and Fe we have adopted for the MEKAL model are 0.1, 1.6, 0.13, 0.22, 0.13, and 0.13 times the solar values (Anders & Grevesse 1989), respectively.

Using the above nebular abundances for single-temperature MEKAL models, it is possible to reproduce the bulk spectral shape with a plasma temperature of  $kT \sim 0.1$  keV (or  $T \sim 1.1 \times 10^6$  K). To improve the spectral fits and to search for the possible existence

---

<sup>5</sup>Several distances to HD 50896 have been reported, ranging from  $0.6 \pm 0.4$  kpc measured by *Hipparcos* (Perryman et al. 1997) to  $\geq 1.8$  kpc determined from interstellar absorption lines (Howarth & Schmutz 1995). We have critically examined the data from the latter work and conclude that the interstellar absorption convincingly demonstrates that HD 50896 cannot be closer than 1 kpc, ruling out the near distance by *Hipparcos*. The systemic velocity of S 308, derived from the average velocity near the nebular center, and the average velocities of the neighboring H II regions S 303 and S 304 are all near  $V_{\text{LSR}} = 20 \pm 2$  km s<sup>-1</sup> (Chu et al. 1982). The kinematic distance estimated from this radial velocity and the Galactic rotation is  $1.5 \pm 0.2$  kpc. The photometric distance to HD 50896 is  $1.0 \pm 0.2$  kpc (van der Hucht 2001). Combining the latter three distances, we decide to adopt a distance of  $1.5 \pm 0.3$  kpc to HD 50896.

of hotter gas expected from a shocked fast wind, we have also fit the observed spectrum with two temperature components. Only a small improvement is achieved, as the reduced  $\chi^2$  of the single-temperature and two-temperature best fits are  $\chi^2/\text{DoF} = 1.12$  and  $1.02$ , respectively. The best-fit single-temperature model and the low-temperature component of the best-fit two-temperature model are virtually indistinguishable from each other; thus only the best-fit two-temperature MEKAL model is overplotted on the EPIC/pn spectrum in Fig. 3. The absorption column density is  $N_{\text{H}} = 1.1 \times 10^{21} \text{ cm}^{-2}$ ; the temperatures, normalization factors, observed fluxes, and unabsorbed fluxes of these two temperature components are summarized in Table 1. The low temperature component has an accurate temperature and dominates the X-ray emission, while the high temperature component is not well constrained in temperature because it is weak and contributes only 6% of the observed flux, or 1.5% of the unabsorbed flux.

We have also tried spectral fits using MEKAL models with two temperature components and freely varying abundances, and find that the EPIC/pn spectrum can be reasonably well described by temperature components at  $kT_1 = 0.1 \text{ keV}$  and  $kT_2 = 0.7 \text{ keV}$  with N, O, and C abundances at 5.6, 0.37, and 0.3 times solar values, respectively. These abundances are 3–4 times as high, but the N/C ratio ( $\sim 18$  times the solar value) and the temperatures of the two thermal components are similar to those of our best-fit model with fixed nebular abundances. Furthermore, both fixed abundance and freely varying abundance model fits show that the low-temperature component dominates the observed X-ray flux. For a  $1 \times 10^6 \text{ K}$  plasma with collisional ionization equilibrium, N and C exist mainly in He-like ions, and thus the N/C abundance ratio can be constrained by the relative strengths of N VI lines at 0.43 keV and C V lines at 0.3 keV, or the spectral shape below 0.5 keV. The absolute abundances, on the other hand, are not well constrained because the spectral resolution does not allow unambiguous separation of line emission and bremsstrahlung emission. Therefore, we conclude that the diffuse X-ray emission of S 308 originates mostly from N-enriched gas at a temperature of  $\sim 1.1 \times 10^6 \text{ K}$ . This temperature is noticeably lower than the plasma temperatures observed in planetary nebulae or superbubbles (Chu et al. 2001; Guerrero, Gruendl, & Chu 2002; Kastner et al. 2000; Kastner, Vrtilek, & Soker 2001; Dunne et al. 2003; Townsley et al. 2003).

Finally, we have compared our EPIC/pn spectrum of S 308 to Wrigge’s (1999) best-fit model for the *ROSAT* PSPC spectrum. Wrigge’s model consists of two components at temperatures of  $(1.5 \pm 0.1) \times 10^6 \text{ K}$  and  $(2.8 \pm 0.4) \times 10^7 \text{ K}$ , with the high-temperature component contributing about 1/3 of the total X-ray flux. Our EPIC/pn spectrum clearly rules out the presence of this high-temperature component, which may be caused by a combination of a low S/N in the PSPC data and contaminations from the numerous point sources projected within the boundary of S 308. These point sources are resolved by the

*XMM-Newton* EPIC cameras but not the *ROSAT* PSPC detector.

## 5. Discussion

### 5.1. Dynamical Parameters of the S 308 Bubble

S 308 is a bubble blown by the WN4 star HD 50896 (Johnson & Hogg 1965) in a circumstellar medium that was ejected by its progenitor during the RSG phase (Esteban et al. 1992). At a distance of  $1.5 \pm 0.3$  kpc, its  $20'$  radius corresponds to  $9 \pm 2$  pc. The nebular shell of S 308 is photoionized, but additional shock heating is present as the nebular  $[\text{O III}]\lambda 5007/\text{H}\beta$  ratios are as high as  $\sim 20$  (Esteban et al. 1992). The presence of shocks is also evidenced in the nebular morphology at the shell rim where the  $[\text{O III}]$  emission leads the  $\text{H}\alpha$  emission by  $16\text{--}20''$  (Gruendl et al. 2000). The S 308 shell resides inside an H I cavity evacuated by the stellar wind of HD 50896's main-sequence progenitor, with the optical nebulae S 303 and S 304 (Fig. 1a of Chu et al. 1982) as part of the fossil swept-up interstellar shell (Arnal & Cappa 1996). The overall nebular structure and environment of S 308 agree well with the expectations of García-Segura et al.'s (1996) models for WR bubbles.

Assuming that the RSG progenitor had a constant mass loss rate  $\dot{M}_{\text{RSG}}$  and a constant wind velocity  $V_{\text{RSG}}$ , the circumstellar medium of HD 50896 would have a radial density profile  $\propto r^{-2}$ . Assuming further that the WR star has a constant mass loss rate  $\dot{M}$  and a constant terminal wind velocity  $V_\infty$ , the bubble expansion velocity will be constant with

$$V_{\text{exp}} = (\dot{M}V_\infty V_{\text{RSG}}/\dot{M}_{\text{RSG}})^{1/2} \quad (1)$$

(García-Segura & Mac Low 1995). For a shell expansion velocity of  $63 \pm 3$  km s $^{-1}$  (Chu et al. 1982) and a radius of  $9 \pm 2$  pc, the dynamic age of S 308 is thus  $(1.4 \pm 0.3) \times 10^5$  yr. The terminal velocity of HD 50896's fast stellar wind has been well measured to be  $V_\infty = 1,720$  km s $^{-1}$  (Prinja, Barlow, & Howarth 1990). The mass loss rate of HD 50896's fast wind has been determined by Nugis, Crowther, & Willis (1998) from IR and radio continuum measurements assuming a smooth wind or a clumped wind for a distance of 1.8 kpc. With the distance adjusted from 1.8 kpc to  $1.5 \pm 0.3$  kpc, the smooth-wind and clumping-corrected mass loss rates of HD 50896 are  $(3.6 \pm 1.1) \times 10^{-5}$  M $_{\odot}$  yr $^{-1}$  and  $(1.4 \pm 0.5) \times 10^{-5}$  M $_{\odot}$  yr $^{-1}$ , respectively. If we assume that the high electron temperature measured in the nebular shell,  $(1.4 - 1.8) \times 10^4$  K (Esteban et al. 1992), is caused by shock heating, then the shock velocity has to be  $\geq 30$  km s $^{-1}$ . The RSG wind velocity can be approximated by the difference between the shell expansion velocity and the shock velocity, thus  $V_{\text{RSG}} \leq 30$  km s $^{-1}$ ; from Eq. (1) we then find the RSG mass loss rate to be  $\dot{M}_{\text{RSG}} \leq (4.7 \pm 1.4) \times 10^{-4}$  M $_{\odot}$  yr $^{-1}$  for

the case of smooth fast wind, or  $\leq (1.9 \pm 0.6) \times 10^{-4} M_{\odot} \text{ yr}^{-1}$  for the case of clumped fast wind.

The nebular shell of S 308 has a sharp rim, indicating that it is still surrounded by RSG wind material; however, the RSG wind material must not extend much further in radius, as a breakout has already occurred at the northwestern part of the shell. The unperturbed RSG wind material just exterior to the nebular shell was ejected at least  $(2.9 \pm 0.6) \times 10^5$  years ago. As the fast WR wind started  $(1.4 \pm 0.3) \times 10^5$  yr ago, the RSG wind lasted  $(1.5 \pm 0.3) \times 10^5$  yr, and the total RSG mass loss would be  $\leq 70_{-30}^{+45} M_{\odot}$  and  $\leq 29_{-13}^{+15} M_{\odot}$  for the cases of smooth and clumped fast winds, respectively. Evidently, the former value is unrealistically large for a normal massive star; thus the total RSG mass loss confirms Nugis et al.'s (1998) suggestion that the clumping-corrected mass loss rates of WR stars are more accurate. Therefore, we will use only the clumping-corrected mass loss rate for the rest of the discussion. The physical parameters of the RSG progenitor and the nebular shell derived above are summarized in Table 2. Note that the velocity, mass loss rate, and total amount of mass loss of the RSG wind derived from bubble dynamics are all well within the canonical ranges of these parameters, and therefore provide a very satisfactory consistency check for the bubble dynamics.

## 5.2. The Hot Interior of S 308

The *XMM-Newton* observations of S 308 show an X-ray spectrum dominated by emission from a N-enriched medium at a temperature of  $\sim 1.1 \times 10^6$  K, with less than 6% of the observed flux contributed by hotter gas. This dominant temperature is almost two orders of magnitude lower than the post-shock temperature of the  $1,720 \text{ km s}^{-1}$  fast stellar wind,  $\sim 8.3 \times 10^7$  K, for a H/He ratio of 0.2 in the WR wind (Nugis et al. 1998). The cooling time scale for such hot gas is much longer than the dynamic age of the bubble; therefore, the observed low plasma temperature indicates that cool nebular material has been mixed into the shocked WR wind to lower the temperature. This mixing is supported by the limb-brightened X-ray morphology of S 308.

Two known mechanisms can mix nebular material with the hot gas: mass evaporation due to thermal conduction and mass loading due to dynamic ablation. The former mechanism has been incorporated into bubble models of Weaver et al. (1977) and Pittard et al. (2001a), and the latter mechanism has been used by Pittard et al. (2001b). To determine whether evaporation or ablation is responsible for the mixing in S 308, we need to know whether the WR wind is shocked and where the shock front is. In the bubble model of Weaver et al. (1977), the fast stellar wind encounters an inner, stagnation shock and the shocked stellar

wind provides the thermal pressure to drive the expansion of the nebular shell. Thermal conduction at the interface between the hot interior gas and the cool nebular shell evaporates nebular material into the hot interior, but the bulk of the shocked fast wind remains hot and occupies most of the volume in the bubble interior. We may estimate the X-ray emission expected from the “uncontaminated” shocked stellar wind of HD 50896 and compare it to the observed diffuse X-ray emission from S 308. The WR wind of HD 50896 has injected  $2 \pm 1 M_{\odot}$  into the bubble interior during the lifetime of the bubble. If the shocked fast wind is uniformly distributed within the bubble interior (the worst-case scenario for emissivity and detectability), the electron density would be  $0.015 \pm 0.003 \text{ cm}^{-3}$ , for a H/He ratio of 0.2. The total volume emission measure of this shocked wind at  $8.3 \times 10^7 \text{ K}$  can be scaled to determine its expected normalization factor  $A$  (see Table 1 for the definition of the normalization factor) for the aperture with which our EPIC spectrum was extracted; we find an expected normalization factor to be  $(1.2 \pm 0.1) \times 10^{-4} \text{ cm}^{-5}$ . Compared with the two temperature components from the best spectral fit listed in Table 1, the normalization factor expected for the X-ray emission from the uncontaminated shocked wind is fortuitously close to that of the  $T_2$  component. If the hot shocked wind occupies only a fraction of the total volume, the expected normalization factor will be higher and would have been detected by our *XMM-Newton* observation if its useful exposure time was not shortened by a high background. Deeper X-ray observations are needed to place more stringent limits on the existence or absence of the shocked stellar wind at  $8.3 \times 10^7 \text{ K}$ .

We have used the best-fit spectral model to determine the unabsorbed X-ray flux from S 308,  $7.2 \times 10^{-12} \text{ ergs cm}^{-2} \text{ s}^{-1}$  within the  $210 \text{ arcmin}^2$  aperture in the  $0.25\text{--}1.5 \text{ keV}$  energy band. This X-ray flux can be scaled to the entire area covered by the bubble to estimate the total X-ray luminosity. As the observed aperture contains the brightest patch of diffuse X-ray emission within S 308, the X-ray luminosity of S 308 should be  $\leq (1.2 \pm 0.5) \times 10^{34} \text{ ergs s}^{-1}$ . The rms electron density of the X-ray-emitting gas in S 308 can be determined from the normalization factor  $A$  given in Table 1,  $N_e = (0.20 \pm 0.03) \epsilon^{-1/2} \text{ cm}^{-3}$ , where  $\epsilon$  is the volume filling factor of the hot gas. For  $\epsilon = 0.5$ , the rms  $N_e = 0.28 \pm 0.04 \text{ cm}^{-3}$  and the total mass of the hot gas is  $11 \pm 5 M_{\odot}$ ; while for  $\epsilon = 0.1$ , the rms  $N_e = 0.63 \pm 0.09 \text{ cm}^{-3}$  and the total mass of the hot gas is  $5 \pm 2 M_{\odot}$ . As the limb-brightened morphology of the diffuse X-ray emission indicates a thick shell structure, the filling factor must be closer to 0.5 than 0.1. Therefore, the hot gas mass is much larger than the total WR wind mass that has been injected into the bubble interior,  $2 \pm 1 M_{\odot}$ , suggesting that nebular material contributes to the hot gas mass and justifying the fixed nebular abundances we used for the spectral fits in §4.

Our present *XMM-Newton* observations do not detect enough photons to warrant a spatially resolved spectral analysis of S 308. Future deeper observations are needed to determine

the radial temperature structure of the X-ray emitting gas. A complete mapping of S 308 is also needed to determine whether the varying morphology of the optical shell rim coincides with spatial and physical variations in the adjacent hot, X-ray emitting gas in the bubble interior.

### 5.3. Interface between the Hot Interior and the Cool Shell

UV observations in conjunction with X-ray observations of S 308 allow us to probe the interface between the hot gas in the bubble interior and the cool gas in the swept-up shell. High-resolution UV spectra of HD 50896 have detected a nebular N V absorption line component associated with the approaching side of the S 308 shell, and its large column density suggests an overabundance in nitrogen (Boroson et al. 1997). As the ionization potential of N IV is 77.5 eV, N V must be produced by collisional ionization in gas at temperatures of a few  $\times 10^5$  K, which is expected at the interface between the hot interior gas and the cool nebular shell of a bubble. The detection of N V absorption from the S 308 shell has provided the strongest evidence of the existence of an interface layer.

Our *XMM-Newton* X-ray image of S 308 reveals the relative location of the hot interior gas and the cool nebular shell (see Fig. 1d). The projected outer edge of the diffuse X-ray emission is offset from the projected outer edge of the [O III] emission by 90'' to over 200'', corresponding to 0.5 – 1.7 pc. As the [O III] rim depicts the outer shock associated with the swept-up shell advancing into the unperturbed RSG wind, this “gap” contains the swept-up shell and the interface layer where the temperature drops radially from  $10^6$  K to  $10^4$  K. The large angular size of this gap makes it the most promising site where an interface layer may be spatially resolved and studied in detail. Future long-slit high-dispersion spectra of the H $\alpha$  + [N II] lines are needed to determine kinematically the exact width of the swept-up shell. We have been awarded *Far Ultraviolet Spectroscopic Explorer (FUSE)* observations of the O VI emission for three positions in S 308. While these *FUSE* observations of O VI emission may reveal the existence of  $3 \times 10^5$  K gas at the interface, the relatively large aperture (30''  $\times$  30'') provides only modest spatial resolution. Future high-resolution, long-slit *Hubble Space Telescope* STIS UV spectra of the N V and C IV emission lines at the gap are needed to probe the temperature structure in the interface layer. Only through the analysis of these detailed multi-wavelength observations can we finally learn empirically how fast stellar winds interact with the ambient medium and test the various theoretical models of bubbles.

## 6. Summary and Conclusions

We have obtained *XMM-Newton* EPIC observations of the northwest quadrant of the circumstellar bubble S 308 blown by the WN4 star HD 50896. Diffuse X-ray emission is unambiguously detected, showing a limb-brightened morphology with a clear gap extending from the outer edge of the diffuse X-ray emission to the outer rim of the nebular shell. The X-ray spectrum of the diffuse emission is very soft, and is well fitted by an optically thin plasma model for a plasma at temperatures of  $\sim 1.1 \times 10^6$  K. For such a low temperature, the N/C abundance ratio is well constrained by the spectral shape below 0.5 keV; spectral fits with freely varying abundances and fixed nebular abundances show consistently that the N/C ratio of the hot gas in S 308 is 15–20 times the solar value. A hotter component may exist, but its temperature is not well constrained,  $8_{-6}^{+17} \times 10^6$  K, and contributes less than 6% of the observed X-ray flux.

We have applied García-Segura & Mac Low's (1995) analytical model for a WR bubble blown in the progenitor's RSG wind to S 308, using observed bubble dynamics and stellar wind parameters, and derived the masses lost by HD 50896 via the RSG wind and the WR wind. We have also used the X-ray data to determine the mass of the X-ray-emitting gas in the bubble interior. The results are summarized in Table 2. It can be seen that the mass in the hot gas is indeed much larger than the total mass injected by the WR wind, indicating that the hot gas is dominated by the nebular material mixed into the bubble interior. It is not clear whether the mixing is through conductive evaporation or dynamic ablation. Deep X-ray observations are needed to detect hotter gas and to resolve the temperature structure in the bubble interior. Spatially resolved UV spectroscopic observations of the interface between the X-ray-emitting gas and the cool nebular gas are also needed to probe the physical mechanisms that mix the nebular material into the hot interior.

This research was supported by the NASA grant NAG 5-10037.

## REFERENCES

Anders, E., & Grevesse, N. 1989, *Geochim. Cosmochim. Acta*, 53, 197  
Arnal, E. M., & Cappa, C. E. 1996, *MNRAS*, 279, 788  
Balucińska-Church, M., & McCammon, D. 1992, *ApJ*, 400, 699  
Bochkarev, N. G. 1988, *Nature*, 332, 518

Boroson, B., McCray, R., Clark, C. O., Slavin, J., Mac Low, M., Chu, Y., & Van Buren, D. 1997, *ApJ*, 478, 638 [Erratum: 1997, *ApJ*, 485, 436]

Chu, Y.-H., Guerrero, M. A., Gruendl, R. A., Williams, R. M., & Kaler, J. B. 2001, *ApJ*, 553, L69

Chu, Y.-H., Mac Low, M. M., García-Segura, G., Wakker, B., & Kennicutt, R. C. 1993, *ApJ*, 414, 213

Chu, Y.-H., Gull, T. R., Treffers, R. R., Kwitter, K. B., & Troland, T. H. 1982, *ApJ*, 254, 562

Dahlem, M. 1999, XMM Users' Handbook

Dunne, B. C., Chu, Y.-H., Chen, C.-H. R., Lowry, J. D., Townsley, L., Gruendl, R. A., Guerrero, M. A., & Rosado, M. 2003, *ApJ*, 590, 306

Esteban, C., Vilchez, J. M., Smith, L. J., & Clegg, R. E. S. 1992, *A&A*, 259, 629

García-Segura, G., Langer, N., & Mac Low, M.-M. 1996, *A&A*, 316, 133

García-Segura, G., & Mac Low, M. 1995, *ApJ*, 455, 145

Gruendl, R. A., Chu, Y.-H., Dunne, B. C., & Points, S. D. 2000, *AJ*, 120, 2670

Guerrero, M. A., Gruendl, R. A., & Chu, Y.-H. 2002, *A&A*, 387, L1

Hillier, D. J. 1988, *ApJ*, 327, 822

Howarth, I. D., & Phillips, A. P. 1986, *MNRAS*, 222, 809

Howarth, I. D. & Schmutz, W. 1995, *A&A*, 294, 529

Johnson, H. M., & Hogg, D. E. 1965, *ApJ*, 142, 1033

Kaastra, J. S., & Mewe, R. 1993, *Legacy*, 3, 16, HEASARC, NASA

Kastner, J. H., Soker, N., Vrtilek, S. D., & Dgani, R. 2000, *ApJ*, 545, L57

Kastner, J. H., Vrtilek, S. D., & Soker, N. 2001, *ApJ*, 550, L189

Liedahl, D. A., Osterheld, A. L., & Goldstein, W. H. 1995, *ApJ*, 438, L115

Nugis, T., Crowther, P. A., & Willis, A. J. 1998, *A&A*, 333, 956

Perryman, M. A. C. et al. 1997, *A&A*, 323, L49

Pittard, J. M., Dyson, J. E., & Hartquist, T. W. 2001a, *A&A*, 367, 1000

Pittard, J. M., Hartquist, T. W., & Dyson, J. E., 2001b, *A&A*, 373, 1043

Prinja, R. K., Barlow, M. J., & Howarth, I. D. 1990, *ApJ*, 361, 607

Strüder, L. et al. 2001, *A&A*, 365, 18

Townsley, L. K., Feigelson, E. D., Montmerle, T., Broos, P. S., Chu, Y.-H., Garmire, G. P. 2003, *ApJ*, 593, 874

van der Hucht, K. A. 2001, *New Astronomy Review*, 45, 135

Weaver, R., McCray, R., Castor, J., Shapiro, P., & Moore, R. 1977, *ApJ*, 218, 377

Wrigge, M. 1999, *A&A*, 343, 599

Wrigge, M., Chu, Y.-H., Magnier, E. A., & Kamata, Y. 1998, *Lecture Notes in Physics*, v.506, Berlin Springer Verlag, 506, 425

Wrigge, M., Chu, Y.-H., Magnier, E. A., & Wendker, H. J. 2003, *ApJ*, submitted

Wrigge, M., Wendker, H. J., & Wisotzki, L. 1994, *A&A*, 286, 219

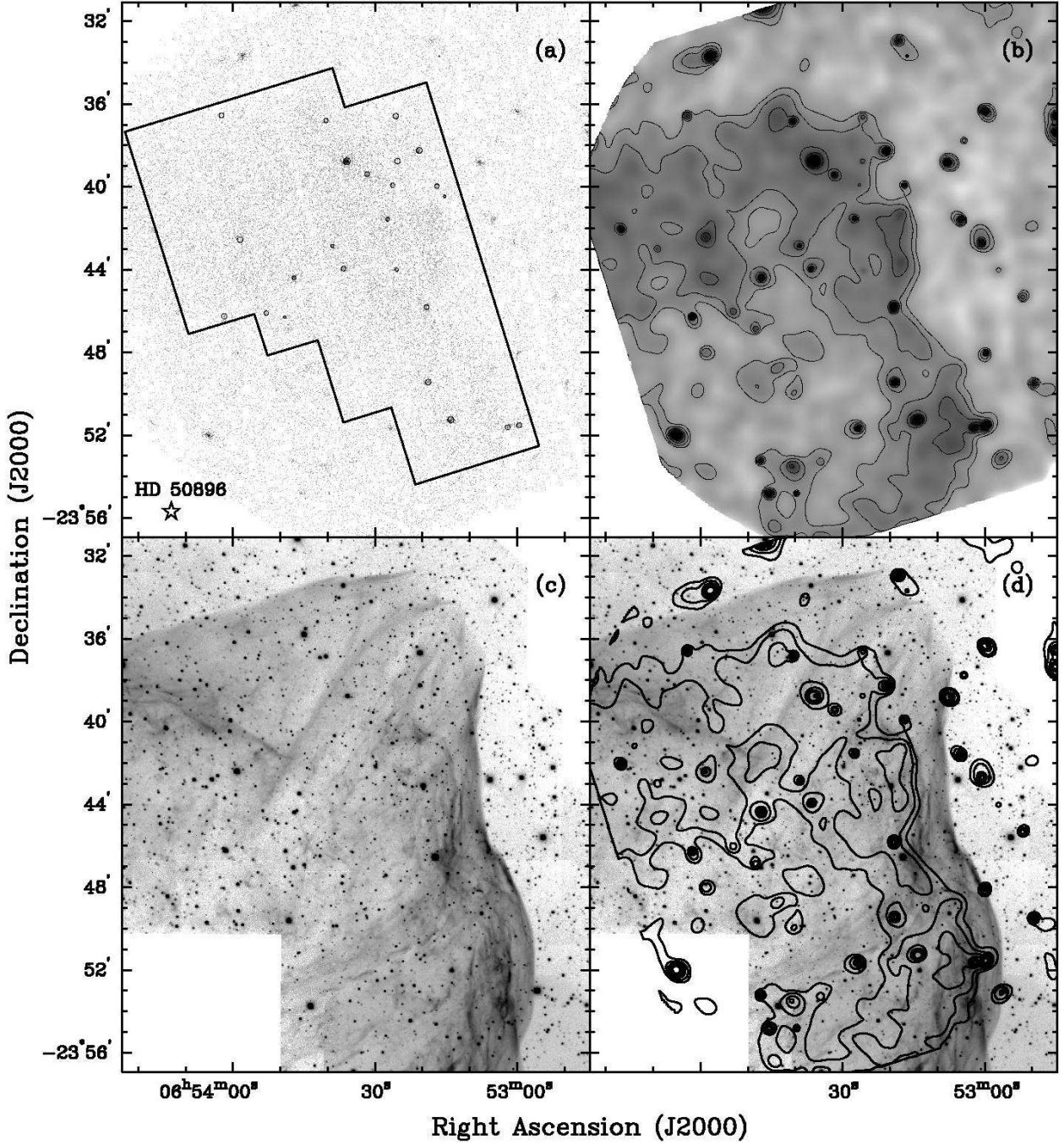


Fig. 1.— (a) *XMM-Newton* EPIC image of the northwest quadrant of S 308. The polygon marks the aperture used to extract spectra of the diffuse X-ray emission. The small circles mark the regions centered on the point sources that have been excluded from the source region when extracting X-ray spectra. The location of HD 50896 is marked. (b) Adaptively smoothed and vignetting corrected X-ray image. The contours levels are at 3, 5, 10, 20, 30, 40, and 50  $\sigma$  above the background. (c) [O III]  $\lambda 5007$  line image of the northwest quadrant of S 308, taken with the Mount Laguna 1m telescope. (d) [O III] image overplotted with X-ray contours.

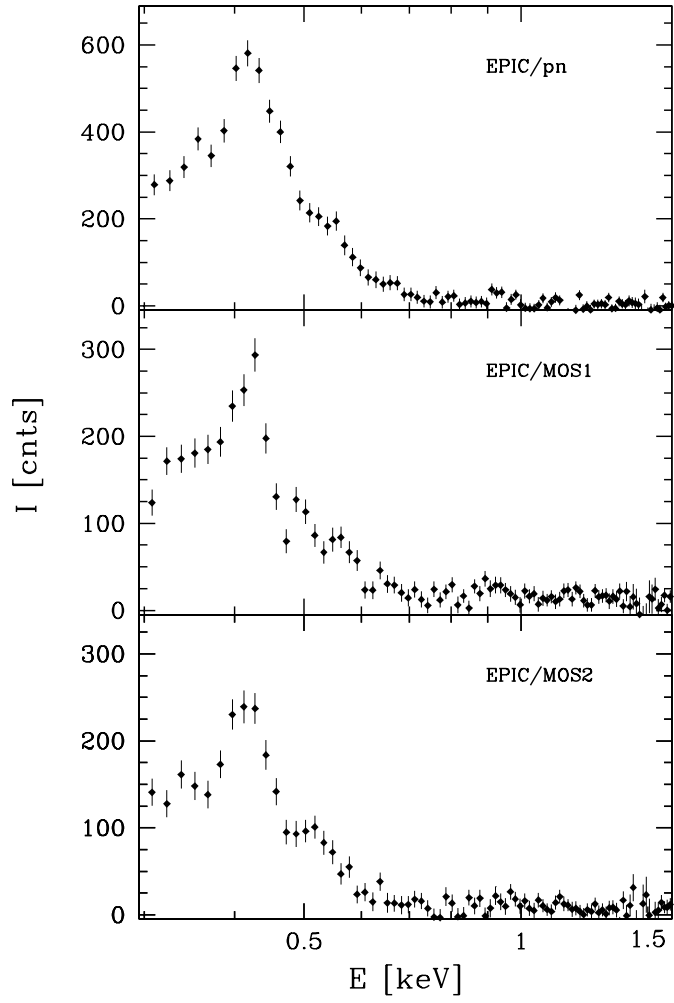


Fig. 2.— *XMM-Newton* EPIC spectra extracted from the pn, MOS1, and MOS2 cameras, respectively.

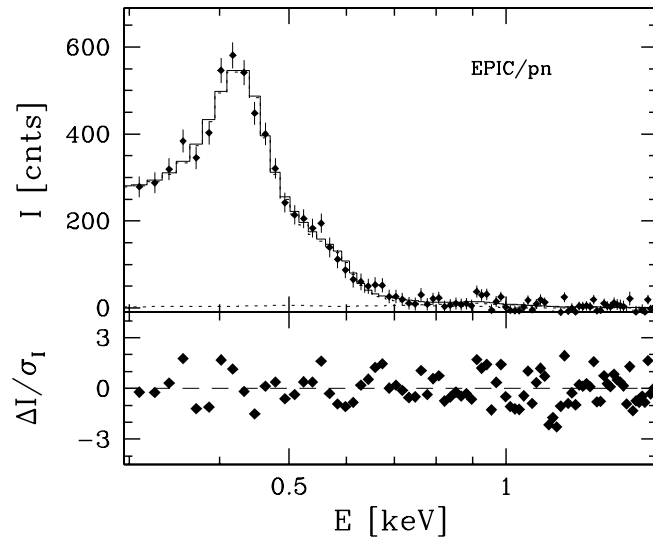


Fig. 3.— *XMM-Newton* EPIC/pn spectrum overplotted with the best-fit model. The solid curve is the best-fit two-temperature model, and the dashed curves are the spectra of individual components. The low-temperature component is so dominant that its spectrum is almost indistinguishable from the sum of both components; it is also virtually indistinguishable from the best-fit of a single-temperature model. The spectrum of the high-temperature component is the dashed curve near the zero line; it contributes 6% of the observed flux, but a negligible number of counts. The bottom panel shows the residuals.

Table 1. Best-fit MEKAL Model for S308

Components	$kT$ (keV)	$A^a$ ( $\text{cm}^{-5}$ )	$f_{0.25-1.5}^{\text{obs}}$ ( $\text{ergs cm}^{-2} \text{ s}^{-1}$ )	$f_{0.25-1.5}^{\text{unabs}}$ ( $\text{ergs cm}^{-2} \text{ s}^{-1}$ )
$T_1$	$0.094 \pm 0.009$	$(2.1 \pm 0.6) \times 10^{-2}$	$1.0 \times 10^{-12}$	$7.2 \times 10^{-12}$
$T_2$	$0.7_{-0.5}^{+1.5}$	$(1.3 \pm 0.8) \times 10^{-4}$	$5.8 \times 10^{-14}$	$1.1 \times 10^{-13}$

<sup>a</sup>  $A = \frac{1.0 \times 10^{-14}}{4\pi d^2} \int N_e^2 dV$ , where  $d$  is the distance,  $N_e$  is the electron density, and  $V$  is the volume in cgs units.

Table 2. Physical Parameters of S308

Parameter	Value	Unit	Reference
Distance	$1.5 \pm 0.3$	kpc	
Radius	$9 \pm 2$	pc	
Expansion velocity ( $V_{\text{exp}}$ )	$63 \pm 3$	$\text{km s}^{-1}$	Chu et al. (1982)
Dynamic age	$(1.4 \pm 0.3) \times 10^5$	yr	
Central star	HD 50896		van der Hucht (2001)
Spectral type	WN4		van der Hucht (2001)
Mass loss rate ( $\dot{M}$ )	$(1.4 \pm 0.5) \times 10^{-5}$	$M_{\odot} \text{ yr}^{-1}$	Nugis et al. (1998) <sup>a</sup>
Terminal wind velocity ( $V_{\infty}$ )	1,720	$\text{km s}^{-1}$	Prinja et al. (1990)
RSG mass loss rate ( $\dot{M}_{\text{RSG}}$ )	$\leq (1.9 \pm 0.6) \times 10^{-4}$	$M_{\odot} \text{ yr}^{-1}$	
RSG wind velocity ( $V_{\text{RSG}}$ )	$\leq 30$	$\text{km s}^{-1}$	
Total RSG wind mass	$29_{-13}^{+15}$	$M_{\odot}$	
Total WR wind mass	$2 \pm 1$	$M_{\odot}$	
$N_{\text{e}}$ of the X-ray-emitting gas:			
$(\epsilon = 0.5)$	$0.28 \pm 0.04$	$\text{cm}^{-3}$	
$(\epsilon = 0.1)$	$0.63 \pm 0.09$	$\text{cm}^{-3}$	
Mass of the X-ray emitting gas:			
$(\epsilon = 0.5)$	$11 \pm 5$	$M_{\odot}$	
$(\epsilon = 0.1)$	$5 \pm 3$	$M_{\odot}$	

<sup>a</sup>This is their clumping-corrected mass loss rate with the distance adjusted from their 1.8 kpc to our  $1.5 \pm 0.3$  kpc.